Amino Acid-Mediated Formation of Zirconia Nanoparticles and their Transparent Dispersions

Amandine Venier, Charlène Brissaud, Benoît Cormary, Erik Camposilvan, Julien Alberici, Denis Chateau, Nora Pousin, Alexandre Chevillot-Biraud, Yannick Millot, Miguel Comesaña-Hermo

Amino Acid-Mediated Formation of Zirconia Nanoparticles and their Transparent Dispersions

*Amandine Venier, Charlène Brissaud, Benoît Cormary, Erik Camposilvan, Julien Alberici, Denis Chateau, Nora Pousin, Alexandre Chevillot-Biraud, Yannick Millot, Miguel Comesaña-Hermo**

Amandine Venier, Benoît Cormary, Erik Camposilvan, Julien Alberici, Denis Chateau, Nora Pousin
Mathym SAS, 69410, Champagne-au-Mont-d'Or (France)

Charlène Brissaud, Alexandre Chevillot-Biraud, Miguel Comesaña-Hermo
Université Paris Cité, CNRS, ITODYS, F-75006 Paris (France)
E-mail : miguel.comesana-hermo@u-paris.fr

Yannick Millot
Sorbonne Université, CNRS, Laboratoire de Réactivité de Surface, LRS, F-75005 Paris (France)

Keywords: zirconia; ceramics; doping; nanoparticles; optical properties

We present a straightforward one-pot hydrothermal method for the synthesis of zirconia nanodispersions, leading to the formation of stable sols. By simply varying the nature of the stabilizer used, one can obtain a large variety of objects with different sizes, shapes and crystallinities. Our results demonstrate the crucial role played by aliphatic amino acids both during the formation of the objects and after, since their interaction with the surface of the inorganic crystals influences strongly the optical properties and colloidal stability of the latter. Importantly, the versatility of this method allows for the introduction of different dopants, increasing substantially the scope of applications that can be achieved with such nanoscale oxides. The high transparencies and the easy dispersibility of nanoparticles in different liquid matrixes ensure the formation of zirconia-based nanocomposites and ceramics with outstanding optical features for the orthopedic, dental, photonics and chemical sectors. This method can be easily scaled up, being already available for the production of high-quality zirconia nanodispersions at the industrial level.

1. Introduction

Zirconia nanoparticles (ZrO_2 NPs) are fundamental building blocks for the development of nanocomposites and ceramics in a broad spectrum of applications, ranging from optics or catalysis to medicine, to name a few.[1–4] On one hand, the high refractive index of ZrO_2 gives the NPs the ability to tune the optical properties of organic materials when used as nanofillers in organic-inorganic nanocomposites. On the other hand, its high melting temperature, superior mechanical strength and extraordinary resistance to corrosion make it particularly appealing for implementation when used as a ceramic in harsh environments such as those operating in combustion engines or certain electrochemical devices, while its outstanding aesthetics enables its use in dental restorations.[5,6] In all these applications, the crystal phase of ZrO_2 is crucial for obtaining the desired properties.

ZrO_2 exhibits three distinct allotropes under atmospheric pressure, the monoclinic phase being the one thermodynamically stable at temperatures under 1170 °C, the tetragonal between 1170 °C and 2370 °C and the cubic at 2370–2750 °C, the latter marking its melting point. In ZrO_2-based ceramics, the tetragonal and cubic allotropes are crucial due to their enhanced thermal, mechanical, and electrical properties, allowing their use in demanding technical applications such as dental implants and restorations or solid fuel cell electrolytes, among others.[6,7] Maintaining these allotropes in a metastable state at room temperature is essential to circumvent the tetragonal-to-monoclinic (t–m) transformation during cooling, which induces microcracking and compromises mechanical integrity.[8–10] Doping ZrO_2 with yttrium, magnesium, calcium or cerium cations prevents this transformation through a charge compensation mechanism. Such phases can also be stabilized below a critical grain size in nanocrystalline ZrO_2 without doping or the presence of impurities, due to thermodynamic considerations.[11,12] Moreover, both the presence of stabilizers and the grain size have an effect on the transformation toughening mechanism, which is responsible for the unique mechanical properties of ZrO_2 ceramics, including high toughness and high strength.[13] Therefore, the final microstructural and mechanical properties of ZrO_2 ceramics can be tuned by leveraging on the synergic effect of grain size and dopant content, which are strictly linked to the chosen synthetic route and the characteristics of the obtained NPs in the initial dispersions.

In the last decades, the scientific community has been particularly focused on the development of synthetic processes for the formation of ZrO_2 NPs.[14–16] This is the result of the improved phase homogeneity and low temperature sintering capabilities of objects at the nanoscale when compared to their bulk counterparts. The formation of ZrO_2 NPs in solution and under mild conditions is preferred over physical methods due to the higher purity, lower cost and the easier

processability of the resulting products. Along these lines, several methodologies have been developed in order to obtain ZrO_2 NPs following chemical routes, allowing for the modulation of the size, shape, chemical composition and surface functionalization of the objects while producing highly crystalline materials, all properties of paramount importance when aiming at the formation of high-performance organic-inorganic nanocomposites and ceramics. Among the different chemical routes available, hydrothermal[17–19] methods are by far the most broadly used for the production of large quantities of ZrO_2-based NPs, given their easy scalability when compared with other approaches.[20–23] Such characteristic is fostered by the high yields obtained and the absence of expensive precursors. Moreover, the use of water as a solvent is particularly appealing since it implies a more sustainable approach, lower costs and an easier processing of the objects, facilitating their implementation in industrial applications. Nevertheless, many hydrothermal methods reported to date include tedious intermediate steps due to the formation of an amorphous zirconium hydroxide ($Zr(OH)_4{\cdot}nH_2O$) after the dispersion of different Zr precursors in a basic medium or the need for a post-synthetic calcination step at high temperatures.[24–29] Moreover, colloidal dispersions obtained following these routes usually lead to partial aggregation of the primary particles in solution, forming larger clusters that have an important impact on the transparency of the sols and nanocomposite dispersions as well as the sinterability of the NPs.[30] Alternatively, the development of hydrothermal treatments at acidic pH has led to the formation of aqueous ZrO_2 nanodispersions with improved optical features.[31] Nevertheless, the development of a versatile and one-pot hydrothermal process in which stable and transparent sols can be achieved is still lacking. With all the above, the development of a scalable colloidal processing methodology allowing a tight control of size and shape together with a versatile modification of the chemical composition and hence crystalline structure of the final objects is an important asset toward their implementation at the industrial scale.

In the present work we introduce a new hydrothermal route for the formation of ZrO_2-based nanodispersions thanks to the use of aliphatic amino acids as stabilizers during the formation of the NPs. Importantly, this procedure leads to the one-pot formation of stable colloidal solutions that maintain extremely high transparency values in the visible and near infrared regions of the electromagnetic spectrum, even at very high solid contents. This last characteristic is of primary importance in the development of organic-inorganic nanocomposites designed for the fabrication of antireflection films, displays or optical fibers. Along these lines, the processability of the dispersions in monomer mixtures while preserving

high transparencies will also be discussed. The high versatility of the process presented herein ensures easy tuning of doping conditions depending on the final applications envisioned, permitting its implementation for the synthesis of other inorganic nanodispersions. Finally, we will also discuss the easy scalability of our protocol at the industrial level.

2. Results and discussion

The inorganic NPs presented in this study have been synthesized following a one-pot straightforward method in which $ZrOCl_2$ and an organic stabilizing agent are dispersed in water with or without a doping agent, being finally submitted to a hydrothermal treatment inside a Teflon-lined stainless steel autoclave. In this manner, four different organic molecules have been chosen as stabilizers: 2-pyrrolidone (P), N-methyl-2-pyrrolidone (N), 4-aminobutanoic acid (C4) and 6-aminohexanoic acid (C6) (see **Scheme S1** in the Supporting Information). Hydrothermal treatment at 200 °C for 3 hours leads to the formation of stable colloidal suspensions in all cases. As can be seen in **Figure 1a-i**, the undoped ZrO_2 NPs present different morphologies depending on the nature of the molecule used as stabilizer, being intimately related to the substantial modulation of the optical features observed (*vide infra*). For instance, the dispersions obtained with P (ZrO_2-P) lead to well-defined anisotropic objects with 20 nm in length while those obtained in the presence of N (ZrO_2-N) produce dendritic structures composed by 3 nm NPs. In comparison, the objects obtained with C4 (ZrO_2-C4) are also anisotropic but much larger, with lengths above 50 nm. Finally, ZrO_2-C6 is composed by a combination of spherical ZrO_2 crystallites of 6 nm in diameter together with larger anisotropic objects such as those obtained in ZrO_2-C4. For more detailed information with respect to the size and shape of the undoped NPs, please refer to **Table S1**. **Figure 2a** presents the XRD patterns of these four samples. Importantly, all the materials obtained following this hydrothermal route are crystalline. More in detail, while the use of P, N and C4 leads to the formation of purely monoclinic phases, C6 leads to a mixture of both monoclinic and tetragonal phases with a 50:50 ratio. The origin of the coexistence of these two phases has been elucidated thanks to HRTEM measurements, showing that in ZrO_2-C6 the anisotropic objects hold a monoclinic structure, while the smaller and almost spherical ones present a tetragonal phase (**Figure 1h, i**). As discussed above, the stabilization of the metastable tetragonal phase at room temperature can come from a decrease of the surface energy contribution below a NP diameter of ca. 10 nm.[12,32] Previous reports have discussed that different parameters such as reaction temperature,[33] precursor concentration[34] or the presence of different chemical species at the surface of the NPs[35] can affect the crystalline structure of ZrO_2 NPs obtained through colloidal

chemistry routes. As discussed below, the different steric hindrance of the molecules used in the present study during the nucleation and growth steps and the chemical interaction between their functional groups and the inorganic surface can also be at the origin of the different morphologies and sizes obtained, thus influencing the final crystalline structures of the objects. Interestingly, the Scherrer equation applied to the XRD diffractograms shows that the ZrO_2 NPs present larger crystalline domains when C4 and C6 are used as stabilizers, in comparison to the domains obtained for P and N samples (**Table S1**).

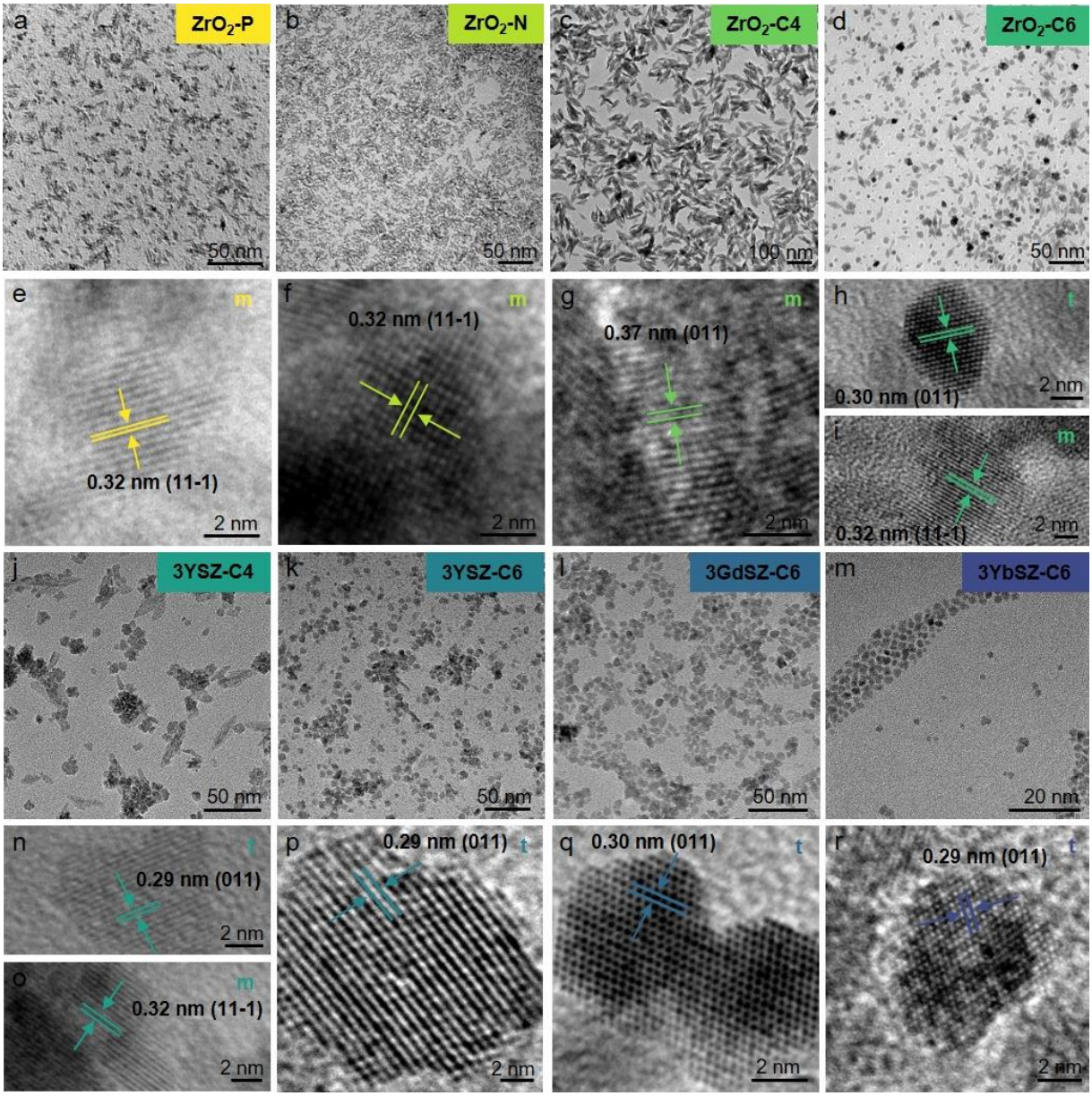

Figure 1. (a-r) TEM and HRTEM characterization of ZrO_2 NPs obtained with the different organic stabilizers and in the presence or absence of dopants. The crystalline character of the objects is indicated in the top right corner of each HRTEM image with m referring to monoclinic and t to tetragonal crystalline structures.

As presented in the Introduction, doping of ZrO_2 powders has long been considered as the easiest means to avoid the t–m transformation and control the mechanical properties of ceramic components obtained from them. Accordingly, the development of a synthetic protocol that permits the inclusion of other elements within the native crystalline structure of ZrO_2 is a characteristic of paramount importance in order to ensure the formation of ZrO_2-based ceramics with high mechanical strengths and a broader applicability. Therefore, we have repeated the same hydrothermal treatment in the presence of either transition metals (Y) or lanthanides (Gd and Yb), while using C4 or C6 as organic stabilizers. In opposition to the undoped samples, here the presence of isotropic objects with mean diameters below 10 nm is the major feature observed by TEM (**Figure 1j-r**). Only ZrO_2 doped with 3 mol.% Y^{3+} and stabilized by C4 (3YSZ-C4) presents a mixture of spherical and anisotropic NPs. Such result may come from the less efficient steric hindrance obtained with the shorter hydrocarbon chain of C4 in comparison with C6, the latter allowing the stabilization of NPs with higher surface to volume ratios. As discussed above for ZrO_2-C6, the different morphological features observed in 3YSZ-C4 present diverse crystallinities: while the isotropic objects hold a tetragonal structure (**Figure 1n**), the needle-like NPs present a monoclinic one (**Figure 1o**). Indeed, weak diffractions at 28° and 31° corresponding to the monoclinic NPs can be observed in the diffractogram (**Figure 2b**) with a 80:20 ratio between the tetragonal and monoclinic phases. Along these lines, the different surface energies associated with each specific exposed facet for the monoclinic and tetragonal allotropes may also play a role on the final morphological features of the objects. The other three samples (3YSZ-C6, 3GdSZ-C6 and 3YbSZ-C6) are composed by small NPs with tetragonal structure, this result being consistent both with their sizes and the presence of dopants. For more detailed information with respect to the size and shape of the doped NPs, please refer to **Table S2**.

One of the most important advantages of our synthetic procedure relies on its simplicity and high versatility. This last characteristic makes it particularly appealing as a universal technique for the formation of metal oxide nanodispersions. As an example, we have implemented the same protocol for the synthesis of CeO_2 NPs, while expanding the doping of ZrO_2 NPs to other cations such as Ce^{4+}, Ca^{2+} and Mg^{2+}, with different molar ratios (**Table S3**). In all cases we obtain satisfactory results in terms of crystallinity and morphology control while obtaining stable sols directly after the hydrothermal treatment. Another important advantage of this process resides in its cost-efficiency given the absence of post-synthetic treatments, the short reaction time and the relatively mild reaction conditions used. Indeed, the relatively low

temperatures of the hydrothermal treatment and the absence of ammonia lead to a low autogenic pressure inside the reactor, thus rendering the scalability particularly straightforward and less expensive since the cost and gradual wear of the reactor are directly linked to these two parameters. Along these lines, we have been able to implement this protocol at the industrial scale without a negative effect on the properties of the materials obtained with respect to the laboratory-scale setup. Currently, this process can be produced in reactors with capacities close to 100 L, allowing a yield of several kg of dried product per batch. As highlighted in **Figure S1** for 8YSZ-C6, scaling-up the synthesis does not produce a noticeable modification of the structural and morphological features of the NPs. In the same vein, the optical features of the dispersions remain practically unchanged.

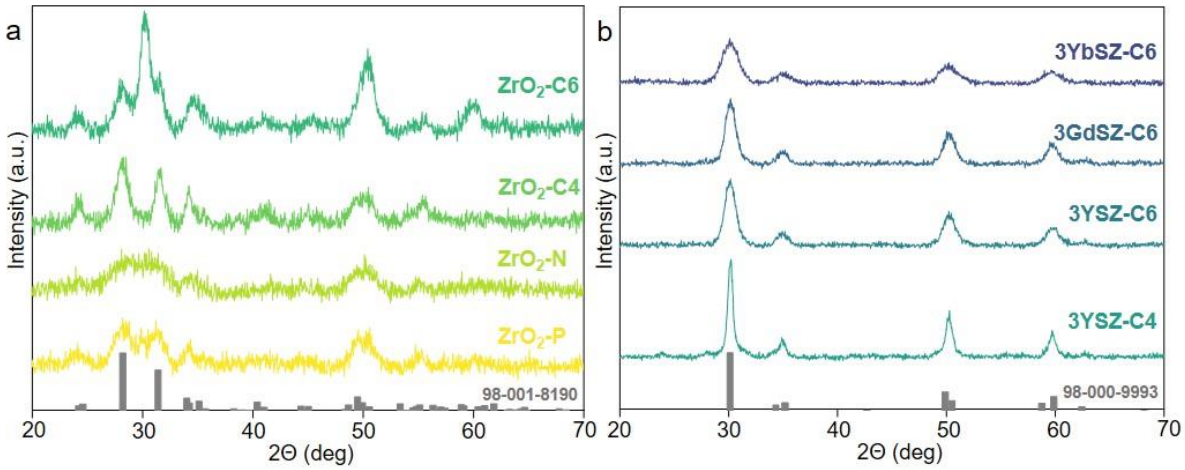

Figure 2. XRD patterns of the undoped (a) and doped (b) ZrO_2 NPs. Reference patterns of the diffractograms for both monoclinic and tetragonal phases (98-001-8190 and 98-000-9993, respectively) are also included.

Two of the materials presented herein (ZrO_2-P and ZrO_2-N) have been obtained in the presence of 5-atom ring cyclic amides or γ-lactams given that previous studies have taken advantage of this family of molecules for the synthesis of transition metal oxide NPs.[36–38] Amides are the least reactive of the carboxylic acid derivatives due to the strong stabilization provided by the donating ability of the lone pair in the nitrogen atom. Nevertheless, lactams can be hydrolyzed under the temperatures and acidic pH of the hydrothermal treatment reported herein, leading to the ring opening and the formation of aliphatic amino acids.[39] For instance, if the lactam P was to be hydrolyzed during the hydrothermal treatment, the ring opening would lead to the formation of C4. Such scenario could be related to the ability of P and N to stabilize ZrO_2 NPs, assuming that the carboxylic acid and/or the amine groups of the amino acids play a major role

during the synthetic process and the subsequent stabilization of the sols. In order to verify this assumption, we have performed IR spectra on free P, free C4, ZrO_2-P and ZrO_2-C4 samples. Free P presents a strong signal at 1674 cm^{-1} that is ascribed to the vibration of the carbonyl group (dark grey spectrum in **Figure S2**). Nevertheless, when the molecule is used to synthesize ZrO_2 NPs, only an extremely weak signal can be observed in the same spectral region. The IR spectrum of free C4 presents a signal at 1574 cm^{-1} corresponding to the asymmetrical stretching vibration of COO^- that can also be observed for both ZrO_2-P and ZrO_2-C4, shifted to a slightly lower value (1543 cm^{-1}) (yellow and green spectra in **Figure S2**, respectively). This finding suggests at least partial hydrolysis of the lactam, with the subsequent ring opening and the formation of an aliphatic amino acid.

In order to understand the role played by each one of the two functional groups of the linear amino acids in the stabilization of the NPs we have performed solid-state ^{13}C NMR experiments. This technique can provide important information concerning the interaction between the stabilizing ligand and the surface of the objects.[40,41] Solid-state Cross-Polarization Magic-Angle-Spinning (CP-MAS) ^{13}C NMR spectra of free C6, ZrO_2-C6 and 3YSZ-C6 are presented in **Figure 3a**, for which the resonances observed below 50 ppm are associated with the hydrocarbon chain of the amino acid. More importantly, while a single resonance with a chemical shift of 182 ppm is obtained from the C atom in the carboxylate of free C6, two signatures can be clearly observed in the same region for both ZrO_2-C6 and 3SYZ-C6. We believe that such difference comes from the adsorption of the carboxylate onto the surface of the oxide NPs, indicating probably the presence of two different coordination modes. Previous results have shown that the resonances observed here at 183 and 175 ppm (**Figure 3b**) could be explained by the formation of chelating and bridging coordination modes between aliphatic carboxylates and the ZrO_2-based NPs, respectively.[42] When performing the same spectra with ZrO_2-P NPs, we also observe the presence of two signatures for the same C atom (**Figure S3**), corroborating that the molecules adsorbed at the surface of the NPs have been previously hydrolyzed to form the aliphatic amino acid, while the concomitant presence of non-hydrolyzed lactams in solution cannot be excluded. It is important to highlight that both resonances are visible after several washing steps of the samples, signifying the strong interaction between the carboxylate moiety and the surface of the objects. In parallel to this, solid-state CP-MAS ^{15}N NMR spectra of free C6 and ZrO_2-C6 have been obtained, showing the presence of a single resonance in both cases at the same position (**Figure S4**). This result suggests that the nitrogen atom of the aliphatic amino acid is still chemically bond to the protons. In the same vein, DLS

experiments performed on diluted suspensions of ZrO_2-C6 and 3YSZ-C6 NPs show their positive surface charge, with ζ–potential values above +25 mV. Such surface state is associated with the protonated character of the amino group within the amino acid adsorbed at the surface of the NPs (pK_a = 10.75), endowing them with sufficient charge to account for the electrostatic repulsions responsible for the high colloidal stability observed. Similar values have been obtained for the other materials presented in this study.

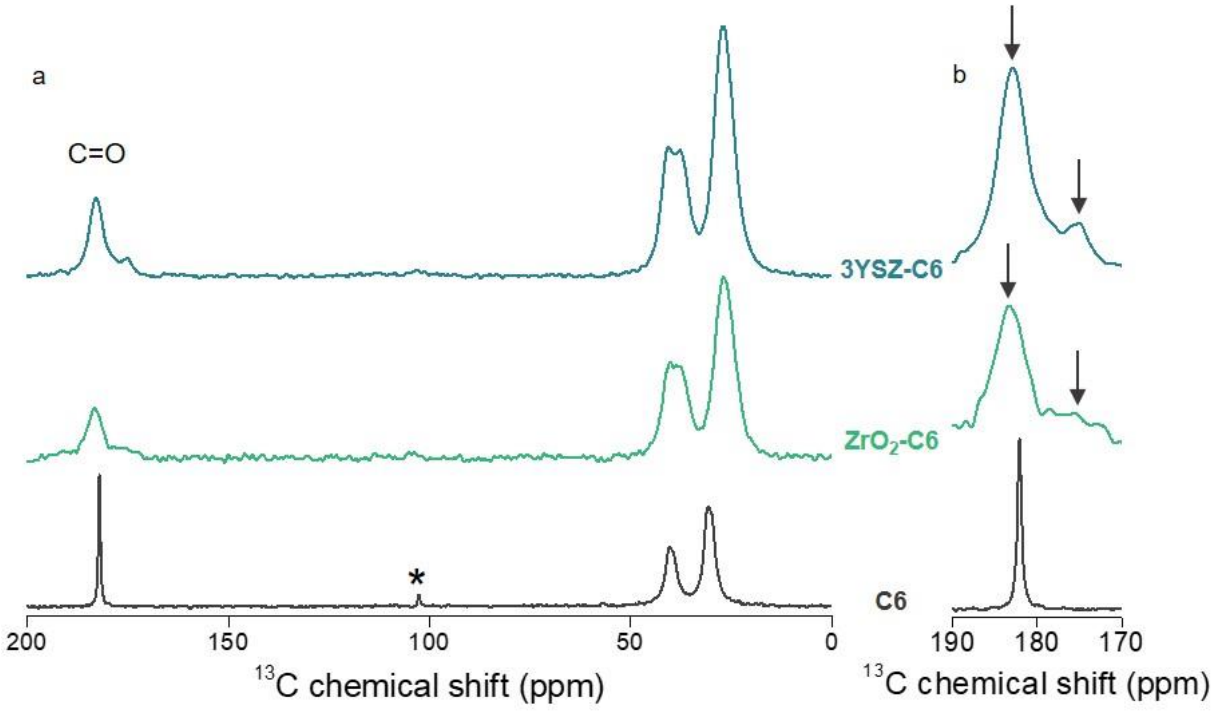

Figure 3. (a) Solid-state CP-MAS ^{13}C NMR spectra of free C6, ZrO_2-C6 and 3YSZ-C6 NPs. (b) Zoom of the region of the carboxylate group resonance where the two signals centered at 183 and 175 ppm can be observed for ZrO_2-C6 and 3YSZ-C6 NPs. The peak identified by * in the free C6 spectrum corresponds to a spinning sideband.

We have also performed several control experiments to demonstrate that the presence of both carboxylic acid and amine functionalities is mandatory in order to obtain stable colloidal suspensions of NPs with controlled morphological and crystallographic features (**Table S4**). For instance, the use of pyrrolidine, a cyclic amine, leads to large aggregates through the formation of a hydroxide intermediate at basic pH. Similar outcomes are obtained with an aliphatic amine. In the same vein, the use of carboxylic acids such as butanoic acid or glutamic acid also leads to unsatisfactory results, with the formation of unstable dispersions of large aggregates. This last result proves that the formation of an acidic dispersion prior to the hydrothermal system and the adsorption of carboxylate moieties at the surface of the crystals

do not suffice to produce stable sols of small NPs. When both an aliphatic amine (butylamine) and a carboxylic acid (butanoic acid) are used in equimolar amounts, unstable and amorphous solids are obtained, highlighting that the double functionality of amino acids is mandatory in order to achieve materials with the desired properties. In parallel, other control experiments have been performed with shorter amino acids than those presented in this study. Accordingly, the use of glycine (C2) and β–alanine (C3) lead to formation of large and irregular aggregates. Such result was expected when taking into consideration that both ZrO_2-C4 and 3YSZ-C4 already present an important population of relatively large objects that have a detrimental effect on the final optical features of the dispersion (*vide infra*). We believe that shorter aliphatic chains lead to the formation of larger objects during the synthesis, thus favoring the formation of monoclinic phases. Moreover, C2 and C3 cannot endow the NPs with enough steric hindrance to ensure the formation of well-dispersed objects in solution, even in the presence of protonated ammonium groups that could participate in the colloidal stabilization via electrostatic repulsions. These control experiments exemplify the interplay between the two functionalities of the amino acids and the importance of the size of their aliphatic chains in order to permit a good control over the morphology of the inorganic NPs and the stabilization of their colloidal solutions. With all the above we conclude that the carboxylic acid group of the aliphatic amino acid is responsible for the chemical interaction with the metal oxide surface, while the protonated amine group endows the NP with high colloidal stability in aqueous solution due to electrostatic repulsions. The chain length of the ligand plays a major role during the synthesis and also contributes to the colloidal stability.

As discussed before, the formation of ZrO_2-based organic-inorganic films and composites with high transparencies are essential for many applications, for instance in the dental or photonics sectors. In an analogous fashion, highly transparent nanodispersions lead to high quality raw materials for the processing of defect-free ceramics with superior properties and smaller microstructures, which are key parameters for improving the aesthetics of the material. Accordingly, dispersions of small NPs such as those presented in this work are particularly appealing. The optical properties of the different dispersions are displayed in **Table 1**. Two general trends can be observed. Firstly, the dispersions stabilized with C4 present the lowest transmittances in the visible range, probably due to the presence of the largest anisotropic objects (ca. 50 nm) in these solutions when compared to the other samples (**Figure 4a**). In opposition to this, those dispersions presenting pseudo-spherical objects with sizes below 10 nm and dendritic structures with relatively short lengths composed by small units present the

highest transmittances across the visible and near infrared regions of the electromagnetic spectrum. For instance, ZrO_2-N, 3YSZ-C6, 3GdSZ-C6 and 3YbSZ-C6 present all transmittances above 90 % when measured at 700 nm for concentrations as high as 40 wt.% (**Figure 4a**). It is important to remark that ZrO_2-P shows particularly high transparencies when compared with ZrO_2-C4, in accordance with the important difference in NP size between both samples (**Figure 1**). We ascribe such difference in morphology to the presence of non-hydrolyzed lactam moieties in the reaction medium during the initial formation of the NPs. These molecules could also partially stabilize the formation of the objects through the interaction between their carbonyl groups and the metal centers during the nucleation process.[37]

Table 1. Transmittance (%) of the different zirconia dispersions in water as a function of the excitation wavelength and solid content. Quartz cuvettes of 1 cm path have been used for all measurements.

Sample	λ: 400 nm 10 wt.%	λ: 600 nm 10 wt.%	λ: 700 nm 10 wt.%	λ: 800 nm 10 wt.%	λ: 400 nm 40 wt.%	λ: 600 nm 40 wt.%	λ: 700 nm 40 wt.%	λ: 800 nm 40 wt.%
ZrO_2-P	62.7	93.2	96.4	97.8	15	68.7	81.4	88.5
ZrO_2-N	72.1	94.8	97	98.1	31.4	85.7	92.2	95
ZrO_2-C4	0.8	6.5	14.9	28.8	0.2	3.4	7.4	15.5
ZrO_2-C6	59.2	89.1	93.2	95.4	28.1	77.5	86.6	91.6
3YSZ-C4	1.6	12.4	28.1	46.1	0.6	2.9	15.6	34.2
3YSZ-C6	64.6	93.1	96.4	97.8	23.1	81.8	91.4	95.8
3GdSZ-C6	64.1	93.1	96.5	98.3	44.2	88.3	93.9	96.6
3YbSZ-C6	80.8	95.6	97.5	98.5	56.4	87	91.4	94.1

The doping of ZrO_2 NPs with 3 mol% Y^{3+} in the dispersions obtained in the presence of C4 and C6 leads to an increase in the transmittance (**Table 1**). For instance, dispersions of 3YSZ-C6 NPs present outstanding transparency values due to the small particle size, low polydispersity and the extremely high colloidal stability endowed by the aliphatic amino acid. As expected, doping ZrO_2 with even higher concentrations of Y_2O_3 leads to a further increase in the transmittance of such dispersions. As an example, we show in **Figure S5** the appearance of a 60 wt.% dispersion of fully-stabilized 8YSZ-C6 NPs, where the outstanding transparency features can be clearly observed. This superior transparency can surely be of interest in optical applications. Nonetheless, when thinking about a technical ceramic body, a higher stabilization

(Y^{3+} content higher than 3 mol%) is often undesirable since this concentration represents the optimum dopant content that allows obtaining the best mechanical properties thanks to the transformation toughening mechanism. This is true at least for conventional ZrO_2 ceramics obtained from sub-micron powders. A higher dopant content is usually accompanied by a decrease in the mechanical strength and an increase in the transparency of the ceramic body.[3,43]

In **Figure 4b** are represented the transmittance spectra of the two doped aqueous dispersions with the highest and lowest degrees of transparency in the region of interest with a solid content of 40 wt.%. On one hand, the 3GdSZ-C6 dispersion presents an extraordinary transparency across the entire visible range that is just slightly superior to the 3YSZ-C6 one, achieving 93.9% transmittance at 700 nm. On the other hand, the dispersion of 3YSZ-C4 presents a very opaque appearance, with only 15.6% transmittance at the same wavelength. As discussed before, here the inefficient steric hindrance offered by the shorter amino acid leads to the formation of an important population of relatively large and anisotropic clusters of monoclinic NPs.

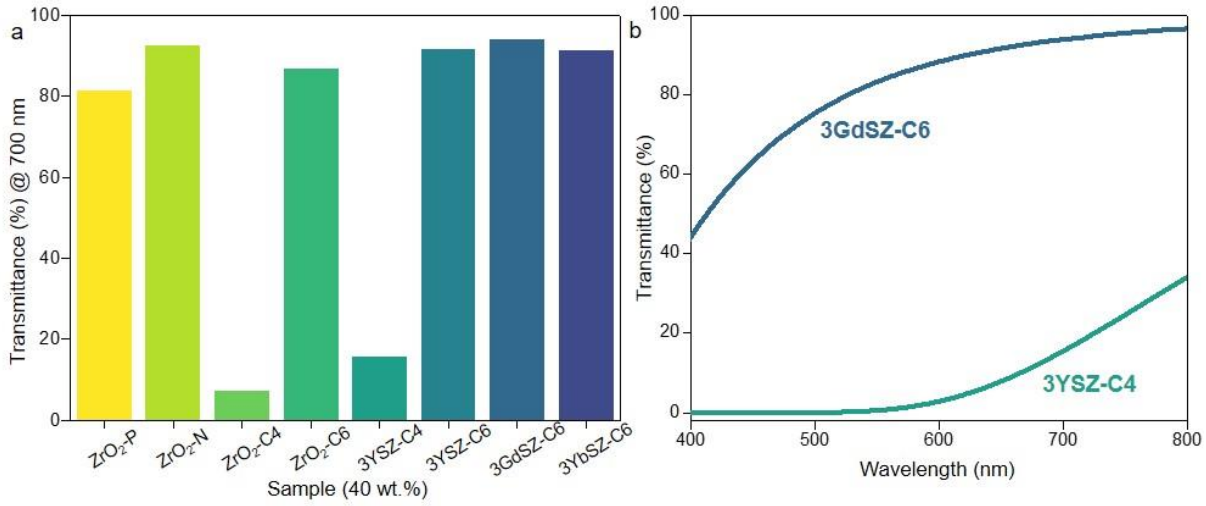

Figure 4. (a) Transmittance values of aqueous dispersions of the different NPs with a concentration of 40 wt.% measured at 700 nm. (b) Transmittance spectra of 3GdSZ-C6 and 3YSZ-C4 at 40 wt.%, the two doped samples with the highest and lowest transparencies in the visible and near infrared ranges of the electromagnetic spectrum, respectively.

The dispersions presented above have been implemented as starting materials for the formation of transparent thin nanocomposite films in order to demonstrate their potential for the integration in coating materials. In optical applications and especially in thin film coating for lenses, transparency must be maximized while the level of haze has to be maintained as low as possible. 8YSZ-C6 NPs have been functionalized with a new grafting ligand in order to be transferred into an acrylate matrix. The chosen acrylate monomer, 1,6-hexanediol diacrylate (HDDA), is a bifunctional acrylate ester monomer used in different fields for the formation of

hybrid inorganic-organic thin films.[44] Here, the monomer has been loaded with different solid contents of 8YSZ NPs (30 wt.% and 50 wt.%), prior to its deposition onto a glass substrate, being finally polymerized in the presence of a photoinitiator under UV irradiation. In **Table 2** are detailed the optical features of the hybrid thin films obtained, with haze values for the functionalized monomers that are almost identical to those obtained from pure acrylate matrixes. More precisely, only a residual increase on haze of 0.1% (within the experimental error of the measurement) is observed (**Figure S6**).

Table 2. Optical features of thin films obtained by the incorporation of 8YSZ-C6 NPs in a polymeric matrix.

Composition	Solid loading (wt.%)	Spinning conditions (rpm)	Film thickness (μm)	Haze (%)
8YSZ-HDDA	30	750	3.0	0.2
8YSZ-HDDA	30	750	3.4	0.1
8YSZ-HDDA	50	750	3.1	0.2
8YSZ-HDDA	50	750	3.2	0.2
HDDA	0	750	2.5	0.1
HDDA	0	750	2.3	0.1

3. Conclusion

In this work, we have presented the straightforward synthesis of ZrO_2-based NPs by means of a one-pot hydrothermal approach in which inorganic precursors are solubilized in the presence of amino acids or lactams that undergo a ring-opening hydrolysis. In this manner, we can obtain a broad library of NP compositions, shapes and crystalline structures by simply modulating the nature and amount of the cation and organic molecule used as dopant and colloidal stabilizer, respectively. The presence of aliphatic amino acids in the reaction mixture seems to stabilize the inorganic NPs through the carboxylate moiety, with the protonated amine providing with outstanding colloidal stability in aqueous solutions. Interestingly, the obtained colloidal dispersions present exceptional optical features with high transparencies in the visible and near infrared regions of the electromagnetic spectrum, even at high solid contents. We believe that such NPs will find an important niche of applications as nanofillers in organic-inorganic composites used in optical applications such as antireflective coatings for displays and lenses and as either raw materials or sintering additives in ceramics for a large range of uses such as dental implants and restorations, solid oxide fuel cells, ceramic fibers and nanofiltration membranes, among others.

4. Experimental Section/Methods

Chemicals: zirconyl chloride hydrate ($ZrOCl_2 \cdot xH_2O$) (99,99%), yttrium (III) chloride hexahydrate ($YCl_3 \cdot 6H_2O$) (99,99%), gadolinium (III) chloride hexahydrate ($GdCl_3 \cdot 6H_2O$) (99,99%), ytterbium (III) chloride hexahydrate ($YbCl_3 \cdot 6H_2O$) (99,9%), 2-pyrrolidone (99%), N-methyl-2-pyrrolidone (99%), 4-aminobutanoic acid (99%) and 6-aminohexanoic acid (98,5%) were all purchased from Sigma-Aldrich and used as received. Distilled water was used for all the preparations.

Synthesis of the ZrO_2-based nanodispersions: 0.036 moles of the inorganic precursors together with 0.119 moles of the chosen organic stabilizer are dispersed in water for a final volume of 72 mL. The mixture is introduced in a Teflon-lined stainless steel autoclave (100 mL) together with a magnetic stirring bar, while the temperature is monitored by connecting a thermocouple to the external wall of the autoclave. The reactor is then introduced in a heated oven at 200 °C and left under magnetic stirring at this temperature for three hours. Lower temperatures (180 °C) or shorter reaction times (1 hour) lead to a partial decrease in the transparency of the sols for some of the formulations (**Table S5**), while longer ones (12 hours) do not have any positive effect on the outcome of the reactions. After this, the reactor is cooled down to room temperature. In order to purify the product of the reaction, the NPs are subjected to cross-flow filtration in distilled water. This technique allows for a continuous depletion in the concentration of molecular impurities by passing the dispersion containing the NPs through a porous (polymeric or ceramic) membrane. The size of the pores allows to eliminate ionic and organic impurities in the permeate while blocking the NPs. In order to obtain a pure dispersion at high concentration, the operation is carried out three times on the feed solution. The yield at the end of the reaction is always > 98 % for all the formulations. For detailed information concerning the characterization of the different samples, please refer to **Table S1** and **Table S2**. Alternatively, more information concerning the reaction conditions (temperature, time, pressure) can be found elsewhere.[45]

Preparation of thin films: Purified aqueous 8YSZ-C6 NPs were functionalized in a volatile organic solvent using a proprietary process and grafting agent, and purified using cross-flow filtration, to obtain a concentrated dispersion of grafted 8YSZ NPs in organic solvent (50 wt.% of dry matter). Typically, 10 g of this 50 wt.% dispersion was mixed with 4,8 g of HDDA and 0,2 g of diphenyl(2,4,6-trimethylbenzoyl)phosphine oxide (TPO) as photoinitiator, and then concentrated under reduced pressure to obtain a solvent-free dispersion of 8YSZ in HDDA at 50 wt.% of NPs. The dispersion of 8YSZ in HDDA at 30 wt.% was prepared by diluting with more HDDA.

These dispersions were filtered on a 1-2µm glass fiber filter and spin coated at 750 rpm. The resulting films were then cured using a LED source (λ = 365 nm) with a power of 3 W for 30s under nitrogen atmosphere.

Characterization: TEM and HRTEM images were obtained using a JEOL 2100+ transmission electron microscope operating at an acceleration voltage of 200 kV. XRD diffractograms were obtained using a Panalytical X'pert pro diffractometer equipped with a Co anode (λKα = 1.79031 Å) and a multichannel X'celerator detector. Visible−NIR spectra were obtained with a Perkin Elmer Lambda 1050 spectrometer using quartz cuvettes with a 1 cm path. Haze measurements were performed on a Jasco V-770 spectrophotometer equipped with a 60 mm diameter integration sphere. FT-IR spectra were recorded with a Nicolet iS50 spectrometer from Thermo Scientific. Solid-state CP-MAS NMR experiments were performed on a Bruker Avance 500 spectrometer with 11.7 Tesla magnets with 7 and 4 mm zirconia rotors, spinning at 6 and 10 kHz, respectively. The resonance frequency of ^{1}H, ^{15}N and ^{13}C were 500.16 MHz, 50.72 MHz and 125.78 MHz, respectively. Chemical shifts (δ) for ^{15}N and ^{13}C were reported relative to glycine powder (33.4 ppm) and adamantane powder (38.52 ppm), respectively. ^{15}N CPMAS spectra were recorded with a contact time of 10 ms and a π/2 pulse duration for ^{1}H of 4.15 µs. Recycle delay and height power decoupling were 3 s and 60 kHz, respectively.^{13}C CPMAS spectra were recorded with a contact time of 1.5 ms and a π/2 pulse duration for ^{1}H of 2.95 µs. Recycle delay and height power decoupling were 5 s and 85 kHz, respectively.

Supporting Information

Supporting Information is available from the Wiley Online Library or from the author.

Conflict of Interest

The methods presented in this work are the basis for the patent FR3089136A1/ US20220009790A1 and the commercial product zilight®, both owned by Mathym SAS.

Acknowledgements

The authors thank Christian Ricolleau and Guillaume Wang at MPQ laboratory (Université Paris Cité) for providing access to their high-resolution transmission electron microscope and Jean-Yves Piquemal (Université Paris Cité) for critical reading of the manuscript. M. C.-H. acknowledges CNRS for financial support.

References

[1] A. Krell, T. Hutzler, J. Klimke, *J. Eur. Ceram. Soc.* **2009**, *29*, 207.

[2] M. N. Tsampas, F. M. Sapountzi, P. Vernoux, *Catal. Sci. Technol.* **2015**, *5*, 4884.

[3] E. Camposilvan, R. Leone, L. Gremillard, R. Sorrentino, F. Zarone, M. Ferrari, J. Chevalier, *Dent. Mater.* **2018**, *34*, 879.

[4] C. Piconi, G. Maccauro, *Biomaterials* **1999**, *20*, 1.

[5] M. H. Bocanegra-Bernal, S. Diaz de la Torre, *J. Mater. Sci.* **2002**, *37*, 4947.

[6] I. Denry, J. R. Kelly, *Dent. Mater.* **2008**, *24*, 299.

[7] M. Ghatee, J. T. S. Irvine, *Int. J. Hydrogen Energy* **2010**, *35*, 9427.

[8] R. C. Garvie, R. H. Hannink, R. T. Pascoe, *Nature* **1975**, *258*, 703.

[9] J. Chevalier, A. Liens, H. Reveron, F. Zhang, P. Reynaud, T. Douillard, L. Preiss, V. Sergo, V. Lughi, M. Swain, N. Courtois, *J. Am. Ceram. Soc.* **2020**, *103*, 1482.

[10] J. Chevalier, L. Gremillard, S. Deville, *Annu. Rev. Mater. Res.* **2007**, *37*, 1.

[11] S. Shukla, S. Seal, *Int. Mater. Rev.* **2005**, *50*, 45.

[12] K. Sato, H. Abe, S. Ohara, *J. Am. Chem. Soc.* **2010**, *132*, 2538.

[13] P. F. Becher, M. V. Swain, *J. Am. Ceram. Soc.* **1992**, *75*, 493.

[14] G. Skandan, H. Hahn, M. Roddy, W. R. Cannon, *J. Am. Ceram. Soc.* **1994**, *77*, 1706.

[15] R. Di Monte, J. Kašpar, *J. Mater. Chem.* **2005**, *15*, 633.

[16] F. Gonell, D. Portehault, B. Julián-López, K. Vallé, C. Sanchez, A. Corma, *Catal. Sci. Technol.* **2016**, *6*, 8257.

[17] W. Li, H. Huang, H. Li, W. Zhang, H. Liu, *Langmuir* **2008**, *24*, 8358.

[18] R. Si, Y. W. Zhang, S. J. Li, B. X. Lin, C. H. Yan, *J. Phys. Chem. B* **2004**, *108*, 12481.

[19] W. Qin, L. Zhu, *Sci. Rep.* **2020**, *10*, 13904.

[20] J. Joo, T. Yu, Y. W. Kim, H. M. Park, F. Wu, J. Z. Zhang, T. Hyeon, *J. Am. Chem. Soc.* **2003**, *125*, 6553.

[21] R. Pokratath, L. Lermusiaux, S. Checchia, J. P. Mathew, S. R. Cooper, J. K. Mathiesen, G. Landaburu, S. Banerjee, S. Tao, N. Reichholf, S. J. L. Billinge, B. Abécassis, K. M. Ø. Jensen, J. De Roo, *ACS Nano* **2023**, *17*, 8796.

[22] G. Garnweitner, L. M. Goldenberg, O. V. Sakhno, M. Antonietti, M. Niederberger, J. Stumpe, *Small* **2007**, *3*, 1626.

[23] P. Stolzenburg, A. Freytag, N. C. Bigall, G. Garnweitner, *CrystEngComm* **2016**, *18*, 8396.

[24] Y. Zhang, Y. Zhao, T. Otroshchenko, S. Han, H. Lund, U. Rodemerck, D. Linke, H. Jiao, G. Jiang, E. V. Kondratenko, *J. Catal.* **2019**, *371*, 313.

[25] G. Dell'Agli, G. Mascolo, M. C. Mascolo, C. Pagliuca, *J. Cryst. Growth* **2005**, *280*, 255.

[26] J. Lin, J. Duh, *J. Am. Ceram. Soc.* **1997**, *80*, 92.

[27] S. Wang, Y. Zhai, X. Li, Y. Li, K. Wang, *J. Am. Ceram. Soc.* **2006**, *89*, 3577.

[28] C. V. Reddy, I. N. Reddy, K. R. Reddy, S. Jaesool, K. Yoo, *Electrochim. Acta* **2019**, *317*, 416.

[29] H. Dan, L. Chen, Z. Li, X. He, Y. Ding, *Inorg. Chem. Commun.* **2022**, *138*, 109272.

[30] K. Sato, K. Horiguchi, T. Nishikawa, S. Yagishita, K. Kuruma, T. Murakami, H. Abe, *Inorg. Chem.* **2015**, *54*, 7976.

[31] H. S. Lee, H. Ko, K. Heo, H. Lee, H. M. Lim, *Colloids Surfaces A Physicochem. Eng. Asp.* **2023**, *670*, 131476.

[32] R. C. Garvie, *J. Phys. Chem.* **1978**, *82*, 218.

[33] T. A. Cheema, G. Garnweitner, *CrystEngComm* **2014**, *16*, 3366.

[34] F. Tana, A. Serafini, L. Lutterotti, A. Cigada, F. Variola, F. Bondioli, L. De Nardo, *CrystEngComm* **2018**, *20*, 879.

[35] X. Jiao, D. Chen, L. Xiao, *J. Cryst. Growth* **2003**, *258*, 158.

[36] Z. Li, H. Chen, H. Bao, M. Gao, *Chem. Mater.* **2004**, *16*, 1391.

[37] Z. Li, Q. Sun, M. Gao, *Angew. Chem. Int. Ed.* **2005**, *44*.

[38] H. Xia, G. Yang, *RSC Adv.* **2013**, *3*, 12320.

[39] P. C. Vollhardt, N. E. Schore, *Organic Chemistry. Structure and Function*, Othe Editi., W. H. Freeman, **2018**.

[40] J. De Roo, *Chem. Mater.* **2023**, *35*, 3781.

[41] L. B. Casabianca, *Solid State Nucl. Magn. Reson.* **2020**, *107*, 101664.

[42] J. De Roo, E. A. Baquero, Y. Coppel, K. De Keukeleere, I. Van Driessche, C. Nayral, Z. Hens, F. Delpech, *Chempluschem* **2016**, *81*, 1216.

[43] J. Chevalier, L. Gremillard, A. V Virkar, D. R. Clarke, *J. Am. Ceram. Soc.* **2009**, *92*, 1901.

[44] H. R. Byun, E. A. You, Y. G. Ha, *Appl. Phys. Lett.* **2019**, *114*, 013301.

[45] A. Venier, E. Camposilvan, M. Comesaña-Hermo, *Method for producing zirconium dioxide nanoparticles in the preence of an amino acid*, **2022**, p. US 2022/0009790 A1.

We present a simple, scalable and versatile hydrothermal method for the formation of zirconia-based nanodispersions with an outstanding control of the morphology, composition and crystalline structure of the objects obtained. Given their optical features, these dispersions can be used as starting materials for the formation of organic-inorganic nanocomposites in a large number of applications.

*Amandine Venier, Charlène Brissaud, Benoît Cormary, Erik Camposilvan, Julien Alberici, Denis Chateau, Nora Pousin, Alexandre Chevillot-Biraud, Yannick Millot, Miguel Comesaña-Hermo**

Amino Acid-Mediated Formation of Zirconia Nanoparticles and their Transparent Dispersions